

Dalton Transactions

Accepted Manuscript

This article can be cited before page numbers have been issued, to do this please use: P. Yang, M. Wang, J. Shen, M. Li, Z. X. Wang, M. Shao and X. He, *Dalton Trans.*, 2013, DOI: 10.1039/C3DT52500G.



This is an *Accepted Manuscript*, which has been through the RSC Publishing peer review process and has been accepted for publication.

Accepted Manuscripts are published online shortly after acceptance, which is prior to technical editing, formatting and proof reading. This free service from RSC Publishing allows authors to make their results available to the community, in citable form, before publication of the edited article. This *Accepted Manuscript* will be replaced by the edited and formatted *Advance Article* as soon as this is available.

To cite this manuscript please use its permanent Digital Object Identifier (DOI®), which is identical for all formats of publication.

More information about *Accepted Manuscripts* can be found in the [Information for Authors](#).

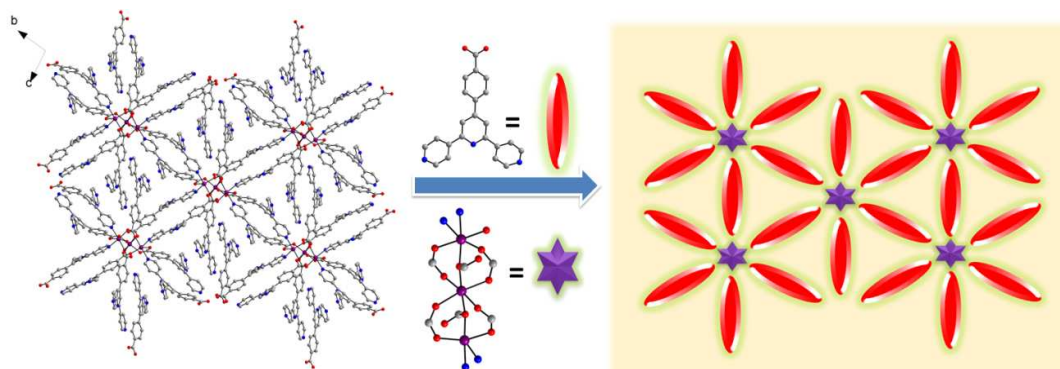
Please note that technical editing may introduce minor changes to the text and/or graphics contained in the manuscript submitted by the author(s) which may alter content, and that the standard [Terms & Conditions](#) and the [ethical guidelines](#) that apply to the journal are still applicable. In no event shall the RSC be held responsible for any errors or omissions in these *Accepted Manuscript* manuscripts or any consequences arising from the use of any information contained in them.

Graphical Abstract

Peng Yang, Meng-Si Wang, Jin-Jin Shen, Ming-Xing Li,* Zhao-Xi Wang, Min Shao, Xiang He*

Seven novel coordination polymers constructed by rigid 4-(4-carboxyphenyl)-terpyridine ligands: synthesis, structural diversity, luminescence and magnetic property

Seven 1D to 3D coordination polymers based on 4/3-Hcptpy ligands were hydro(solvo)thermally synthesized and structurally characterized. The 4/3-Hcptpy ligands display seven types of coordination modes. $[\text{Mn}(4\text{-cptpy})_2]_n$ (**1**) and $[\text{Co}(4\text{-cptpy})_2]_n$ (**2**) are 3D MOFs containing nanosized cavities. $[\text{Mn}_3(4\text{-cptpy})_6(\text{H}_2\text{O})]_n \cdot 2n\text{H}_2\text{O}$ (**3**) possesses a beautiful 2D network assembled by flower-like $\text{Mn}_3(4\text{-cptpy})_6(\text{H}_2\text{O})$ subunits. The complexes **1** and **2** are thermally stable under 440 °C and exhibit antiferromagnetic interactions.



Seven novel coordination polymers constructed by rigid 4-(4-carboxyphenyl)-terpyridine ligands: synthesis, structural diversity, luminescence and magnetic property

Peng Yang,^a Meng-Si Wang,^a Jin-Jin Shen,^a Ming-Xing Li,^{*a} Zhao-Xi Wang,^a Min Shao^b and Xiang He^{*a}

^a Department of Chemistry, College of Sciences, Shanghai University, Shanghai 200444, P. R. China

^b Laboratory for Microstructures, Shanghai University, Shanghai 200444, P. R. China

* Corresponding author. E-mail: mx_li@mail.shu.edu.cn, hxiang@shu.edu.cn

Received (in XXX, XXX) Xth XXXXXXXXXX 200X, Accepted Xth XXXXXXXXXX 200X

10 First published on the web Xth XXXXXXXXXX 200X

DOI: 10.1039/b000000x

Seven coordination polymers, namely $[\text{Mn}(4\text{-cptpy})_2]_n$ (**1**), $[\text{Co}(4\text{-cptpy})_2]_n$ (**2**), $[\text{Mn}_3(4\text{-cptpy})_6(\text{H}_2\text{O})]_n \cdot 2n\text{H}_2\text{O}$ (**3**), $[\text{Co}(4\text{-cptpy})(\text{HCOO})(\text{H}_2\text{O})]_n \cdot n\text{DMF}$ (**4**), $[\text{Zn}_2(4\text{-Hcptpy})_2\text{Cl}_4]_n \cdot 2n\text{C}_2\text{H}_5\text{OH} \cdot n\text{H}_2\text{O}$ (**5**), $[\text{Co}_4(3\text{-cptpy})_4(\text{HCOO})_4(\text{H}_2\text{O})_2]_n$ (**6**), and $[\text{Mn}(3\text{-cptpy})_2]_n$ (**7**) (4-Hcptpy = 4-(4-carboxyphenyl)-4,2':6',4''-terpyridine; 3-Hcptpy = 4-(4-carboxyphenyl)-3,2':6',3''-terpyridine), have been synthesized under hydro(solvo)thermal conditions and structurally characterized. A generally solvothermal method is proposed for preparing carboxylate complexes in DMF solution without any basal additive. **1** and **2** possess isostructural 3D metal-organic frameworks containing nanosized cavities. **3** is a beautiful 2D coordination polymer assembled by flower-like $\text{Mn}_3(4\text{-cptpy})_6(\text{H}_2\text{O})$ subunits. **4** and **6** both display 2D polymeric networks constructed from 4/3-cptpy⁻ ligands, in which the formate ligands originate from the hydrolyzation of DMF. **5** is a 1D 2₁ helical chain polymer. **7** shows a 2D network with a (3.6) two-nodal kgd topology. 4/3-Hcptpy ligands display seven types of coordination modes. Zinc complex **5** emits strong violet luminescence. **1** and **2** are both thermally stable under 440 °C and exhibit antiferromagnetic interactions.

Introduction

Over the past decade, coordination polymers and metal-organic frameworks (MOFs) have attracted intense interest owing to their intriguing structural motifs and potential applications as functional materials.¹ Much effort has been focused on the purposeful design and controllable synthesis of coordination polymers employing multidentate ligands such as polycarboxylate and N-heterocyclic ligands.² Nevertheless, it is still difficult to direct self-assembly process and harvest the desired complexes with objective structures and properties, because many factors can greatly affect the final results, such as the ligand character, metal coordination geometry, reagent ratio, solvent system, pH value, reaction temperature and crystallization method.³ Therefore, it is imperative to further investigate the coordination modes of important multidentate ligands and understand the structure-property relationship inside coordination polymers.

Considering as the most popular ligand in this realm, 4,4'-bipyridine has already been used to construct thousands of complexes.⁴ Moreover, multipyridyl ligands, such as terpyridine and 2,4,6-tris(4-pyridyl)-1,3,5-triazine, are a well-known class of ligands and have found widespread

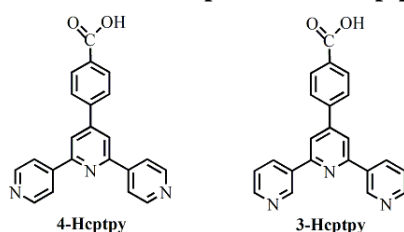
application in constructing MOFs.⁵ As a series of terpyridine derivatives, carboxyphenyl group substituted terpyridine ligands have been received heavy attention for good reasons: a) Advantages of rigid backbone and directional extending ability, which are beneficial to build up porous frameworks possessing good adsorption capacity. b) The extended networks with novel topologies can be constructed based on carboxyphenyl-terpyridine ligands. c) Through multidentate-bridging coordination modes, the introduction of carboxyl group to terpyridine strengthens the capability to assemble diverse discrete metallic polynuclear clusters with potential magnetic interactions. d) With the help of the natural large π -conjugated structures of the carboxyphenyl-terpyridines, materials with active photoluminescence properties could be synthesized. e) The existence of inherent multi-aromatic rings is apt to give rise to π - π stacking interactions, which will play an important role in the formation of supramolecular architectures.

In contrast to the cohesive terpyridyl moiety of 4-(4-carboxyphenyl)-2,2':6',2''-terpyridine (2-Hcptpy) that often acts as a chelating group to assemble complexes with obvious luminescence properties,^{6,7} 4-Hcptpy and 3-Hcptpy (Scheme 1) contain two side exo-pyridyl groups and trend to construct extended high-dimensional coordination

polymers. However, very few efforts were devoted to 4/3-Hcptpy complexes to date.⁸

Overall, the rigid trigonal 4/3-Hcptpy bifunctional ligands possess three pyridyl groups and one carboxylic group, which are valuable multidentate ligands in constructing coordination polymers and porous MOFs. In this paper, seven 4/3-Hcptpy coordination polymers were successfully prepared, in which the 4/3-Hcptpy ligands exhibit versatile coordination modes. The dimensionalities of the entire architectures of the seven complexes vary from 1D to 3D. Herein, we report their syntheses, crystal structures, thermal stabilities, luminescences, and magnetic properties.

Scheme 1. Schematic description of 4/3-Hcptpy ligands



Experimental section

Materials and methods. Reagents and solvents as well as 4/3-Hcptpy ligands employed were commercially available and used as received. Elemental analyses for C, H and N were carried out on a Vario EL III elemental analyzer. IR spectra (KBr pellets) were recorded with a Nicolet A370 FT-IR spectrometer. Thermal analyses were performed on a Netzsch STA 449C thermal analyzer from 20 to 800 °C in N₂ atmosphere. The luminescence spectrum of crystalline sample was recorded on a Shimadzu RF-5301 PC spectrophotometer. Variable-temperature magnetic susceptibilities were measured on a Quantum Design PPMS-9T magnetometer in 2–300 K at a magnetic field of 1000 Oe. The diamagnetic corrections were applied by using Pascal's constants.

Synthesis of [Mn(4-cptpy)₂]_n (1). MnSO₄·H₂O (33.8 mg, 0.2 mmol) was added into a 5 mL H₂O solution containing 4-Hcptpy (35.3 mg, 0.1 mmol) and 1 mL NaOH solution (0.1 mol·L⁻¹). The mixture was sealed in a 15 mL Teflon-lined reactor and then heated at 160 °C for 72 h. The yellow crystals of **1** were obtained in 33% yield based on 4-Hcptpy. Anal. Calcd for C₄₄H₂₈N₆O₄Mn: C, 69.57; H, 3.72; N, 11.06. Found: C, 69.04; H, 4.05; N, 11.28. IR (KBr, cm⁻¹): 3429m, 3072w, 3029w, 1594s, 1565s, 1411s, 1314w, 1215w, 1063w, 1016m, 858w, 825m, 784s, 694m, 632m, 476w.

Synthesis of [Co(4-cptpy)₂]_n (2). The preparation procedure was similar to **1** except that MnSO₄·H₂O was replaced by CoSO₄·7H₂O (56.2 mg, 0.2 mmol). The purple crystals of **2** were obtained in 38% yield based on 4-

Hcptpy. Anal. Calcd for C₄₄H₂₈N₆O₄Co: C, 69.20; H, 3.70; N, 11.00. Found: C, 69.65; H, 4.12; N, 10.58. IR (KBr, cm⁻¹): 3442m, 3072w, 3026w, 1594s, 1563s, 1410s, 1312w, 1063w, 1018m, 859w, 824m, 783s, 695m, 478w.

Synthesis of [Mn₃(4-cptpy)₆(H₂O)_n·2nH₂O (3). A mixture of MnCl₂·4H₂O (19.8 mg, 0.1 mmol), 4-Hcptpy (35.4 mg, 0.1 mmol) and 8 mL H₂O was stirred for 30 min. Then 0.5 mL NaOH solution (0.1 mol·L⁻¹) was added. After stirring for another 30 min, the mixture was sealed in a 15 mL Teflon-lined reactor. The reactor was heated at 160 °C for 72 h, and then cooled to room temperature at a rate of 10 °C h⁻¹. Several yellow crystals of **3** were separated manually from a mixture of white precipitate. Anal. Calcd for C₁₃₂H₉₀N₁₈O₁₅Mn₃: C, 67.95; H, 3.89; N, 10.81. Found: C, 67.87; H, 4.73; N, 11.17. IR (KBr, cm⁻¹): 3419m, 3063w, 1596s, 1550s, 1399s, 1354m, 1065w, 1016m, 861m, 826s, 786s, 695m, 632m, 479w.

Synthesis of [Co(4-cptpy)(HCOO)(H₂O)_n·nDMF (4). A mixture of Co(NO₃)₂·6H₂O (29.1 mg, 0.1 mmol), 4-Hcptpy (35.3 mg, 0.1 mmol) and 8 mL DMF was sealed in a 15 mL Teflon-lined reactor. The reactor was heated at 85 °C for 72 h. The red crystals of **4** were collected in 37% yield based on 4-Hcptpy. Anal. Calcd for C₂₆H₂₄N₄O₆Co: C, 57.05; H, 4.42; N, 10.24. Found: C, 58.57; H, 4.60; N, 9.14. IR (KBr, cm⁻¹): 3418m, 3068w, 2931w, 1662s, 1596s, 1547s, 1390s, 1065w, 1017w, 830m, 787s, 697m, 632m.

Synthesis of [Zn₂(4-Hcptpy)₂Cl₄]_n·2nC₂H₅OH·nH₂O (5). A mixture of ZnCl₂·6H₂O (24.4 mg, 0.1 mmol), 4-Hcptpy (35.3 mg, 0.1 mmol) and 10 mL ethanol was sealed in a 15 mL Teflon-lined reactor. The reactor was heated at 140 °C for 72 h. The light yellow crystals of **5** were collected in 41% yield based on 4-Hcptpy. Anal. Calcd for C₄₈H₄₄Cl₄N₆O₇Zn₂: C, 52.92; H, 4.07; N, 7.71. Found: C, 53.38; H, 3.60; N, 7.66. IR (KBr, cm⁻¹): 3507m, 3067w, 2966w, 2871w, 1684s, 1616s, 1602s, 1539m, 1397s, 1299s, 1217m, 1066s, 1027m, 844s, 774m, 699m, 516m.

Synthesis of [Co₄(3-cptpy)₄(HCOO)₄(H₂O)₂]_n (6). A mixture of Co(NO₃)₂·6H₂O (58.2 mg, 0.2 mmol), 3-Hcptpy (17.6 mg, 0.05 mmol), 3 mL DMF and 3 mL H₂O was sealed in a 15 mL Teflon-lined reactor. The reactor was heated at 120 °C for 72 h. The red crystals of **6** were collected in 46% yield based on 3-Hcptpy. Anal. Calcd for C₉₂H₆₄N₁₂O₁₈Co₄: C, 59.37; H, 3.47; N, 9.03. Found: C, 58.60; H, 3.45; N, 8.79. IR (KBr, cm⁻¹): 3437m, 3066w, 2800w, 1622vs, 1572s, 1389vs, 1353s, 1194m, 1031m, 804s, 784s, 736s, 702s.

Synthesis of [Mn(3-cptpy)₂]_n (7). A mixture of MnSO₄·H₂O (33.8 mg, 0.2 mmol), 3-Hcptpy (35.3 mg, 0.1 mmol), 3 mL dimethylacetamide (DMA) and 3 mL H₂O was sealed in a 15 mL Teflon-lined reactor. The reactor was heated at 120 °C for 72 h. The light yellow crystals of

7 were obtained in 48% yield based on 3-Hcptpy. Anal. Calcd for $C_{44}H_{28}N_6O_4Mn$: C, 69.56; H, 3.72; N, 11.06. Found: C, 68.84; H, 3.07; N, 11.06. IR (KBr, cm^{-1}): 3076w, 1626s, 1570s, 1436m, 1379s, 1164s, 1064m, 1033w, 776s, 732m, 716m.

X-ray crystallography. The single crystals of **1–7** were selected for X-ray diffraction study. Data collections were performed on a Bruker Smart Apex-II CCD diffractometer with graphite-monochromatic Mo $K\alpha$ radiation ($\lambda = 0.71073 \text{ \AA}$) at 293(2) K except **3** at 193(2) K. Determinations of the crystal system, orientation matrix, and cell dimensions were performed according to the established procedures. Lorentz polarization and absorption correction were applied. The structures were solved by the direct methods and refined by full matrix least-squares on F^2 with the SHELXTL-97 program.⁹ All non-hydrogen atoms were refined anisotropically, and hydrogen atoms were located and included at their calculated positions. The crystal data and structural refinement results are summarized in Table 1. The selected bond distances and angles are listed in Table S1 (Electronic supplementary information, ESI). The measured and simulated powder X-ray diffraction patterns are shown in Fig. S1 (ESI).

Results and discussion

Description of the structures

Structures of $[Mn(4\text{-cptpy})_2]_n$ (1**) and $[Co(4\text{-cptpy})_2]_n$ (**2**).** The X-ray structural analysis reveals that complex **1** features a 3D metal–organic framework. As shown in Fig. 1a, the asymmetric unit consists of one independent Mn(II) ion and two 4-cptpy[−] ligands. Mn1 is six-coordinated with a slight distorted octahedral geometry. Four coordination sites on the equatorial plane are occupied by carboxyl O atoms. The axial positions are occupied by two pyridyl N atoms with a N4–Mn1–N1 bond angle of $174.25(11)^\circ$.

Both independent 4-cptpy[−] ligands are tridentate and exhibit different coordination modes. The μ_2 -cptpy[−] ligand coordinates to two Mn(II) ions via a chelating carboxyl group (O3, O4) and an outer pyridyl group (N4) (mode I, Scheme 2). The μ_3 -cptpy[−] ligand combines with three Mn(II) ions through a bridging carboxyl group (O1, O2) and an outer pyridyl group (N1) (mode II, Scheme 2). In each 4-cptpy[−] ligand, four aromatic rings are essentially coplanar. The central pyridyl group and one remaining outer pyridyl group are uncoordinated in order to relieve the steric effect.

It is observed that a Mn_2 dimer is formed as a subunit (Fig. 1b), with the help of the bridging carboxyl group (O1, O2), to build up the framework of **1**. The μ_2 -, μ_3 -cptpy[−]

ligands link Mn(II) ions to assemble a 1D necklace-like polymeric chain with Mn_2 dimers as nodes. This 1D chain is comprised of hexagonal rings with the dimensions of $25.89 \text{ \AA} \times 16.25 \text{ \AA}$ (Mn \cdots Mn distance) in series. With further insight into this structure, it is important to note that mutual parallel 1D chains do not exist in isolation. Specifically, adjacent 1D chains interweave with each other in vertical direction via sharing the metal sites (Fig. 1c). Due to the effective propping originating from the rigid skeleton of 4-cptpy[−] ligands, complex **1** possesses a complicated 3D metal–organic framework that contains nanosized cavities with the dimensions of $16.14 \times 16.86 \times 9.69 \text{ \AA}^3$ (Mn \cdots Mn distance) (Fig. 1d). A more detailed structural analysis indicates that two identical 3D frameworks interpenetrate with each other to give rise to a 2-fold entangled architecture (Fig. S2, ESI). The potential solvent-accessible occupancy volume is 5.5% calculated by PLATON.

The cobalt complex **2** is isostructural with **1**. Both complexes have the similar 3D metal–organic framework. Recently, Wen et al. reported a $[Cd(4\text{-cptpy})_2]_n \cdot 2nDMF$ complex, which is a 2D porous MOF and exhibits selective adsorption of CO_2 and luminescence.^{8a}

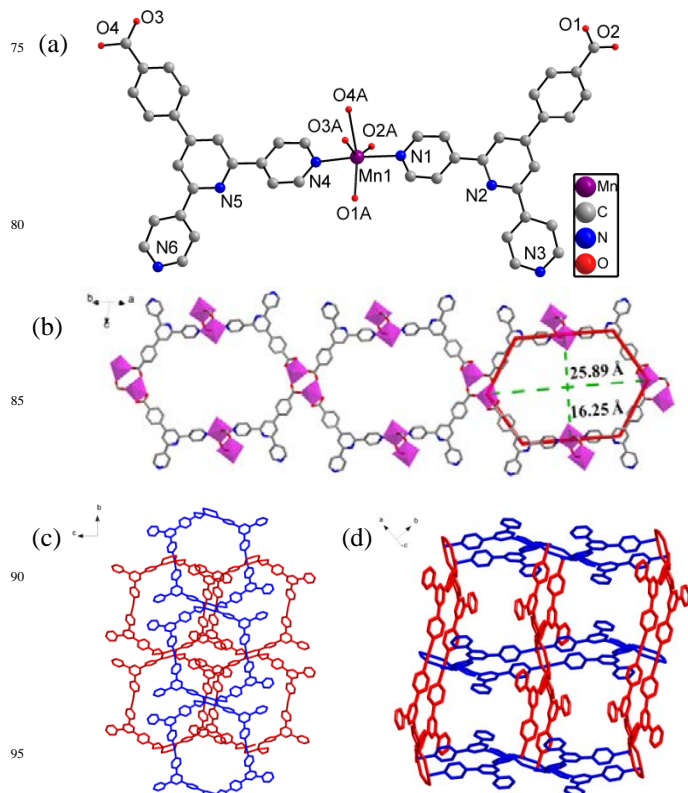


Fig. 1 (a) The asymmetric unit of **1**; (b) the 1D necklace-like chain with Mn_2 dimers; (c) the catena structure; (d) view of the 3D MOF containing nanosized cavities.

Structure of $[Mn_3(4\text{-cptpy})_6(H_2O)]_n \cdot 2nH_2O$ (3**).** Complex **3** is a 2D reticular coordination polymer

constructed from trinuclear Mn(II) clusters. As illustrated in Fig. 2a, the asymmetric unit contains three independent Mn(II) ions, six 4-cptpy⁻ ligands, one coordinated water and two lattice water molecules. Interestingly, six carboxyl groups tightly bind three Mn(II) ions to form a linear Mn₃ cluster that acts as a second building unit for constructing the whole structure of **3** (Fig. 2b). A closer observation reveals that Mn1 and Mn3 both adopt slight distorted octahedral geometries. The former is surrounded by two pyridyl nitrogens, three carboxyl oxygens and water O1W to complete a distorted *cis*-octahedral geometry, while the six coordination sites of Mn3 are all occupied by carboxyl oxygens from six distinct 4-cptpy⁻ ligands. The whole Mn3–O bond distances range from 2.105(5) to 2.380(5) Å. Mn2 is five-coordinated with a distorted triangular-bipyramidal geometry. The axial positions are occupied by carboxyl O7 and pyridyl N8 with a O7–Mn2–N8 bond angle of 175.4(2)°.

Six independent 4-cptpy⁻ ligands display two types of coordination modes, tridentate mode II and bidentate mode III (Scheme 2). Each of four tridentate 4-cptpy⁻ ligands connects three Mn(II) ions via bridging carboxyl group and an outer pyridyl N atom, while each of two bidentate 4-cptpy⁻ ligands connects two Mn(II) ions through one bridging oxygen atom from carboxyl group. On the other hand, six 4-cptpy⁻ ligands could be further divided into three types owing to the different dihedral angles between the phenyl ring and the central pyridyl group (Fig. S3, ESI): a) To reduce the steric hindrance, the dihedral angles of the two 4-cptpy⁻ ligands with central pyridyl N7 and N13 are nearly the same (exhibiting 43.1° and 45.7°, respectively); b) Corresponding dihedral angles in another two 4-cptpy ligands (central pyridyl N1 and N16) range from 20.3° to 25.5°; c) Regarding to the remaining two 4-cptpy⁻ ligands with three free pyridyl groups, four aromatic rings are essential coplanar.

It should be noticed that four bidentate-bridging carboxyl groups and two carboxyl oxygen atoms (O3, O7) fasten Mn1, Mn2 and Mn3 to aggregate a linear trinuclear {Mn₃(μ_{1,3}-CO₂)₄(μ_{1,1}-CO₂)₂} cluster. As far as we know, the analogous {Mn₃O(CO₂)₆} clusters trend to perform

trigonal shape in general.¹⁰ The linear carboxylate-bridged Mn₃ cluster is still rarely reported.¹¹ A more interesting observation is that ten 4-cptpy⁻ ligands around every Mn₃ cluster piece together a beautiful flower-like pattern (Fig. 2c), where Mn₃ cluster is taken as a pistil and 4-cptpy⁻ ligands serve as petals. Among these ten 'petals', two 4-cptpy⁻ anions are terminal ligands, whereas the other eight ones act as bridging ligands. As shown in Figure 2d, neighbouring Mn₃ clusters as subunits are further interconnected by 4-cptpy⁻ bridging ligands to produce a 2D polymeric network containing flower-like (or starfish-like)¹² motifs, in which the shortest distance between the Mn₃ clusters is 16.832 Å (Mn3...Mn3 distance). Such structure is rarely observed before.

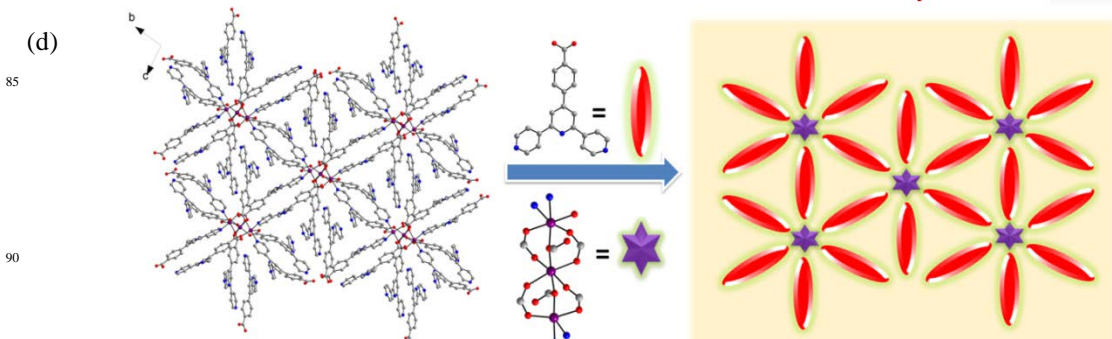
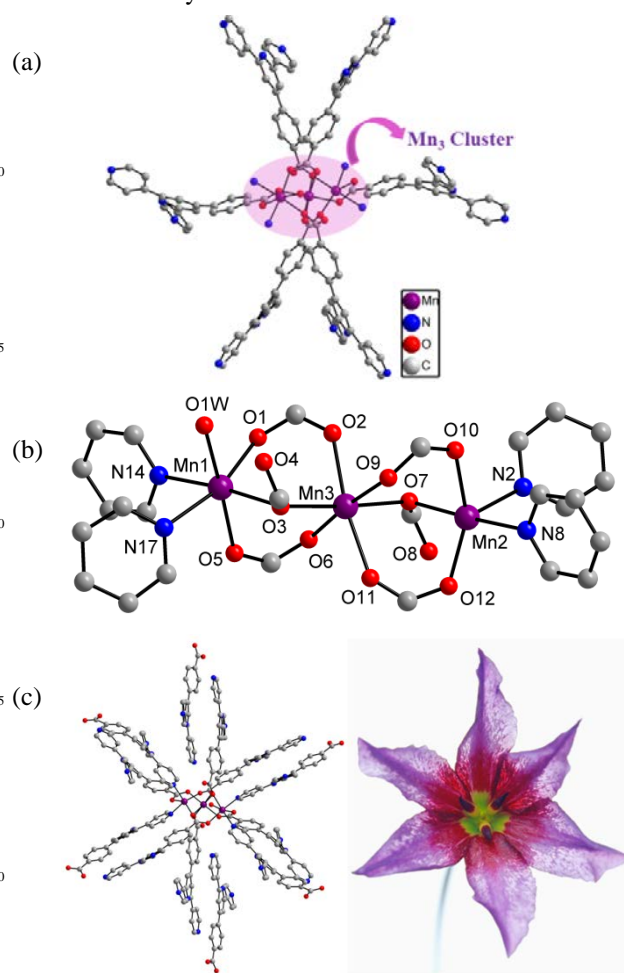


Fig. 2 (a) The asymmetric unit of **3**; (b) the linear carboxylate-bridged Mn_3 cluster; (c) the flower-like pattern of **3**; (d) the 2D polymeric network.

Structure of $[Co(4\text{-cptpy})(HCOO)(H_2O)]_n \cdot nDMF$ (4**).**

The asymmetric unit of **4** consists of one independent Co(II) ion, one 4-cptpy⁻ ligand, one formate ligand, one coordinated water and one lattice DMF molecule (Fig. 3a). It should be noticed that the monodenate $HCOO^-$ ligand originates from the decomposition of DMF at solvothermal conditions.¹³ Co1 adopts a distorted *cis*-octahedral geometry, coordinated by four oxygen atoms and two nitrogen atoms. The chelating carboxyl group (O3, O4) and two pyridyl N atoms (N1, N3) locate at the equatorial plane. The formate O1 and water O1W atoms occupy the axial positions with a O1–Co1–O1W bond angle of 176.9(2)°. As a rigid triangular connector, each 4-cptpy⁻ ligand combines with three Co(II) ions via the chelating carboxyl group and two outer pyridyl groups (mode IV, Scheme 2) to construct a 2D porous network.

As shown in Fig. 3b, 4-cptpy⁻ ligands serve as three-connected spacers, and Co(II) ions serve as three-connected nodes, to generate a hexagonal honeycomb microporous network. The approximate dimensions of the hexagon are 17.75 Å × 12.96 Å. In order to stabilize the whole structure, two 2D porous networks interlace with each other to produce a 2-fold interpenetrating layer (Fig. 3c). Furthermore, the adjacent layers are parallelly packed and interact with each other through hydrogen bond between coordinated water and lattice DMF molecules to generate a supramolecular architecture. Wen et al. reported a complex $\{[Cd(4\text{-cptpy})(Ac)(H_2O)](DMA)(H_2O)\}_n$, which is a 3D porous MOF and exhibits selective adsorption of CO_2 and luminescence.^{8a}

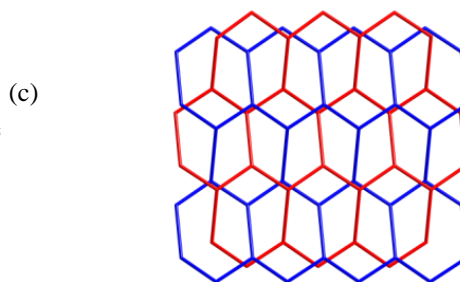
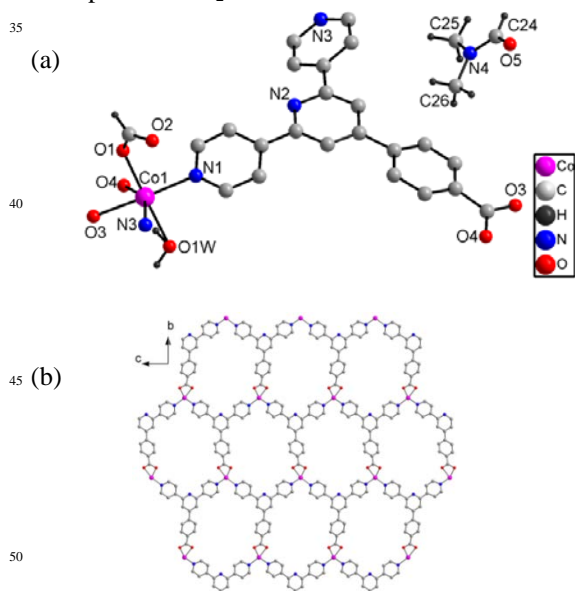


Fig. 3 (a) The asymmetric unit of **4**; (b) the 2D hexagonal honeycomb microporous network along *bc* plane; (c) the 2-fold interpenetrating layer.

Structure of $[Zn_2(4\text{-Hcptpy})_2Cl_4]_n \cdot 2nC_2H_5OH \cdot nH_2O$ (5**).**

Complex **5** possesses a 1D infinite helical chain structure. The asymmetric unit is comprised of two independent Zn(II) ions, two 4-Hcptpy ligands, four Cl^- ligands, two lattice ethanol molecules and one lattice water molecule. As shown in Fig. 4a, both Zn(II) ions are surrounded by two Cl^- ions and two pyridyl N donors, exhibiting similar distorted tetrahedral geometries. The bond angles around Zn1 range from 101.15(17)° to 122.56(8)°, and the bond angles around Zn2 vary from 97.64(18)° to 123.71(10)°. The average Zn–Cl bond distance is 2.22 Å, and the average Zn–N bond distance is 2.06 Å.

Both 4-Hcptpy are neutral and act as bidentate ligands to link two Zn(II) ions via outer pyridyl groups (mode V, Scheme 2). The uncoordinated carboxyphenyl group is twisted by 37.7° with respect to the central pyridyl ring to relieve the steric effect. Careful observation finds that such a connection between the 4-Hcptpy and Zn(II) ions results in two kinds of 1D $[Zn_2(4\text{-Hcptpy})_2Cl_4]_n$ 2₁ helical chains running along the *b*-axis, corresponding to left- and right-handedness (both with a pitch of 14.06(9) Å, Fig. 4b). Additionally, the carboxyl group of 4-Hcptpy remains protonated and interacts via a hydrogen bond (O1–H1A...O2#3 = 2.616(4) Å) with another carboxyl group in adjacent parallel 1D chain to form a 2D supramolecular network with hexagonal rings. Into the same layer, owing to the alternate arrangement of the parallel left- and right-handed helical chains, complex **5** undergoes racemization and crystallizes in an achiral space group, *Pnna*. Furthermore, along different directions, two kinds of weak π – π interactions originate from the neighbouring phenyl rings (centroid-to-centroid distance of 3.910 Å), and pyridyl rings (centroid-to-centroid distance of 3.790 Å) of adjacent helical chains, which further extend the whole structure to a 3D supramolecular framework. (Fig. S4, ESI). Recently, a

1D ribbon polymer $[\text{Zn}(3\text{-cptpy})\text{Cl}]_n$ was reported, in which 3-cptpy⁻ displays tetradentate coordination mode I (Scheme 2).^{8c}

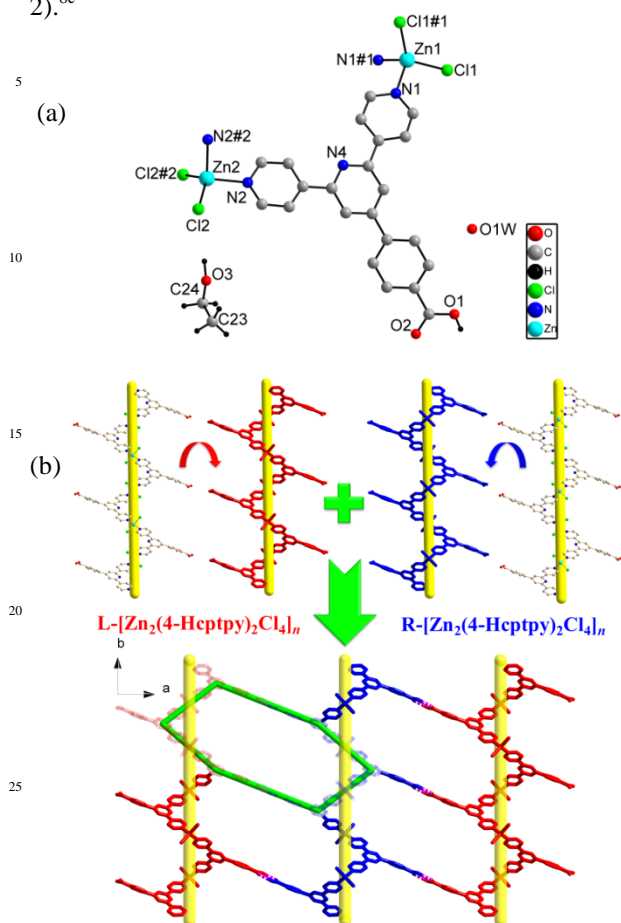


Fig. 4 (a) The asymmetric unit of **5**; (b) perspective view of the 2D supramolecular network built by 1D left- and right-handed helical chains.

Structure of $[\text{Co}_4(3\text{-cptpy})_4(\text{HCOO})_4(\text{H}_2\text{O})_2]_n$ (6**).** Complex **6** is a 3-cptpy-based complex, which possesses a 2D bilayer polymeric network. The asymmetric unit contains four independent Co(II) ions, four 3-cptpy⁻ ligands, four formate ligands and two coordinated water molecules (Fig. 5a). Four distinct Co(II) ions all exhibit *cis*-octahedral geometries with different degrees of

distortion, coordinated by four oxygen atoms and two nitrogen atoms from four disparate 3-cptpy⁻ ligands. As listed in Table S1 (ESI), the bond distances and angles around four cobalt ions are slightly different. All the Co–O bond distances fall in the range of 2.021(9)–2.199(6) Å, and Co–N bond distances vary from 2.162(2) to 2.250(2) Å.

Four 3-cptpy⁻ ligands all serve as tetradentate ligands, each coordinates to four Co(II) ions through bridging carboxyl group and two outer pyridyl groups (mode VI, Scheme 2). Every Co(II) ion is combined with one monodentate formate with an average Co–O bond distance of 2.091 Å. Interestingly, two types of Co₂ dimers $[\text{Co}_2(\text{COO})_2(\text{H}_2\text{O})]$ are formed with the connections of coordinated water and bridging carboxyl groups, brief as 'Co1&Co2' and 'Co3&Co4'. The Co···Co separations are 3.703(6) Å for the former, and 3.655(7) Å for the latter. As connection nodes, these Co₂ dimers are further linked by 3-cptpy⁻ to construct a 2D polymeric network with the shortest distance of 10.502 Å between the Co₂ dimers, as shown in Fig. 5b.

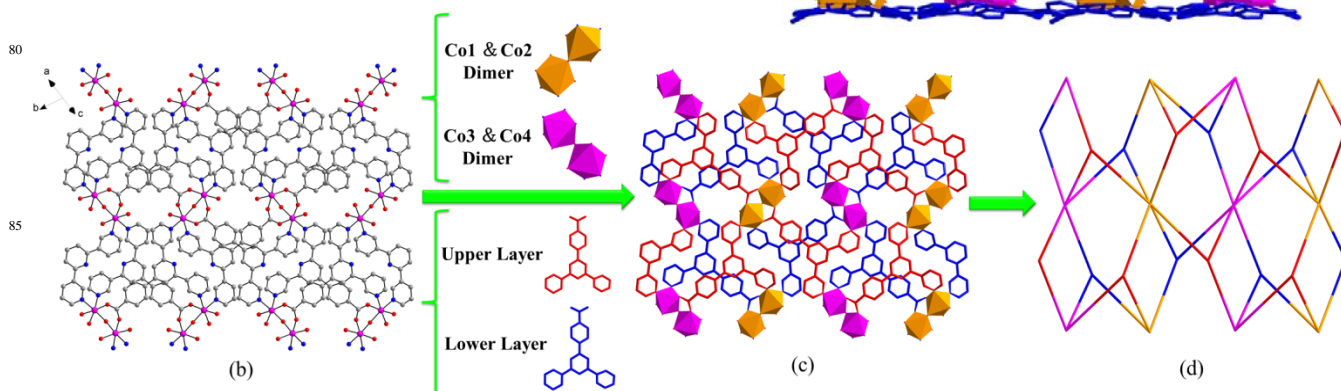
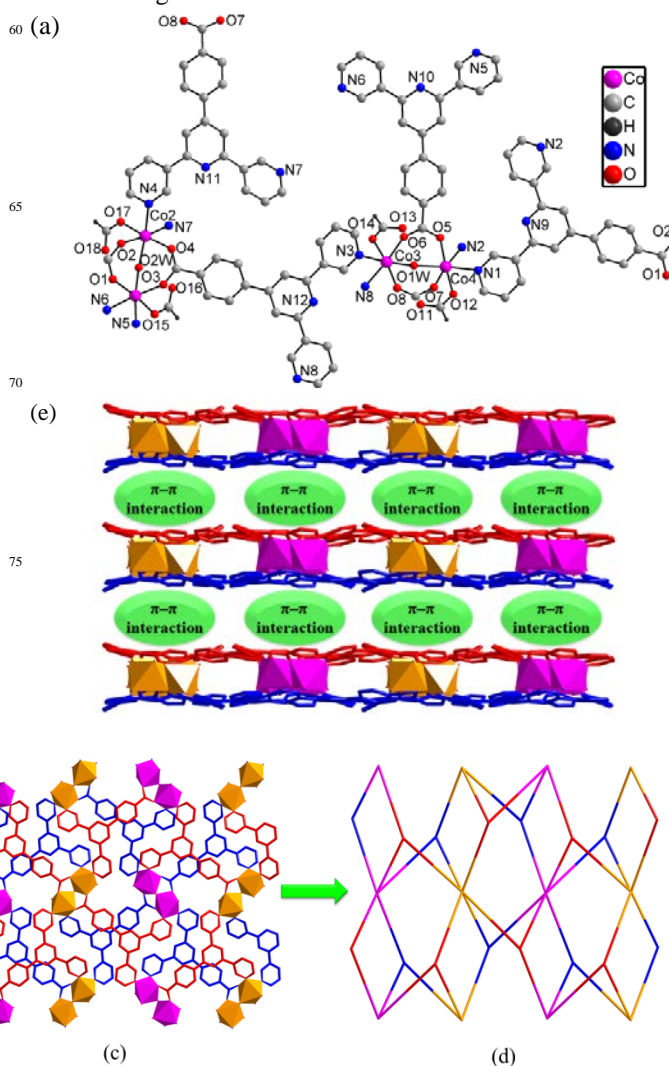


Fig. 5 (a) The asymmetric unit of **6**; (b) perspective view of the 2D polymeric network; (c) the 2D bilayer network of **6**. The 'Co1&Co2 dimer', 'Co3&Co4' dimer, upper layer 3-cptpy⁻, and lower layer 3-cptpy⁻ are marked as orange, pink, red and blue, respectively; (d) the 3.6 two-nodal topology; (e) view of the sandwich-like 3D supramolecular architecture stacking via intermolecular π - π interactions.

Careful observation into this 2D framework indicates that the 3-cptpy⁻ ligands could be classified into two categories, 'upper layer linkers' and 'lower layer linkers', which produce a bilayer network where Co₂ dimers are embedded (Fig. 5c). Regarding two kinds of 3-cptpy⁻ ligands and Co₂ dimers respectively as three-connected and six-connected nodes, the whole framework of **6** can be topologically represented as a (3,6)-connected net with Schläfli symbol $\{4^2.6\}_2\{4^4.6^9.8^2\}$ (Fig. 5d). Ultimately, due to the weak intermolecular π - π stacking interactions from aromatic rings that belong to adjacent layers, these 2D networks are packed into a sandwich-like 3D supramolecule (Fig. 5e).

Structure of [Mn(3-cptpy)₂]_n (7). Complex **7** is a 2D coordination polymer constructed by 3-cptpy⁻ ligand. The asymmetric unit consists of one Mn(II) ion and two 3-cptpy⁻ ligands. As shown in Fig. 6a, Mn1 is six-coordinated with a slight distorted octahedral geometry. The equatorial plane is completed by four O atoms from four bridging carboxyl groups, while the axial positions are occupied by two pyridyl nitrogens with a N1-Mn1-N2 bond angle of 175.17(12)°. The Mn-O bond distances vary from 2.167(3) to 2.196(3) Å, and the average Mn-N distance is 2.313(4) Å.

Both 3-cptpy⁻ ligands are tridentate and adopt the coordination mode VII (Scheme 2). In terms of the steric environment, benzene rings of two distinct 3-cptpy⁻ ligands rotate by nearly the same angles with respect to their central pyridyl groups, presenting 31.0° and 29.5°, respectively. As shown in Fig. 6b, a 2D network is constructed based on the well-organized connection between Mn(II) nodes and 3-cptpy⁻ linkers. The 1D linear Mn polynuclear clusters are included into this 2D network by Mn-(COO)₂-Mn linkages. Acting as unique second building blocks, these metallic clusters combine with pyridyl groups to extend the whole architecture along *bc* plane. To simplify the entire framework into node and connection net, taking 3-cptpy⁻ ligands and Mn(II) ions for three-connected and six-connected nodes respectively, complex **7** exhibits a (3.6) two-nodal kgd topology with the Schläfli symbol $\{4^3\}_2\{4^6.6^8.8^3\}$ (Fig. 6c).

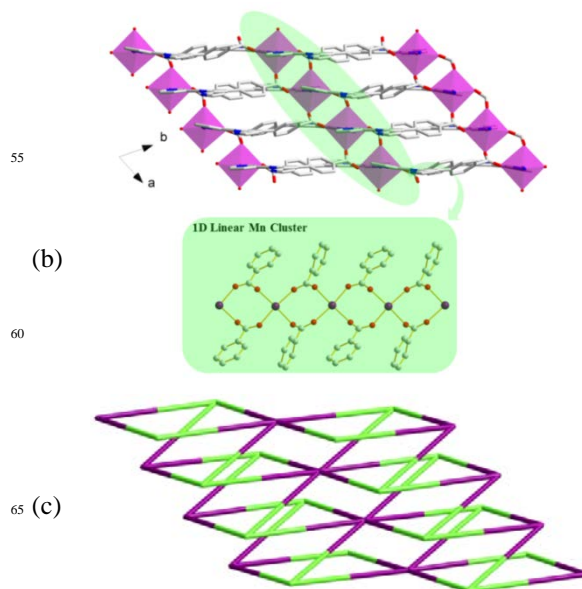
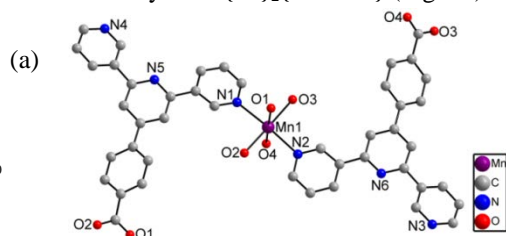
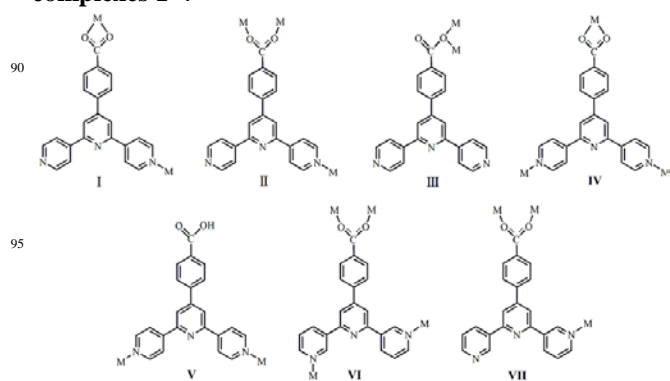


Fig. 6 (a) The asymmetric unit of **7**; (b) perspective views of the 2D network and 1D linear Mn cluster; (c) the 3.6 two-nodal kgd topology. The 3-cptpy⁻ ligands and Mn(II) ions are marked as green and purple, respectively.

Comparison of Hcptpy coordination modes. As summarized in Scheme 2, seven distinct coordination modes of 4/3-Hcptpy, presenting in complex **1-7**, are well depicted. Unlike the 2-Hcptpy, due to the steric hindrance effect, the weak coordination ability of the central pyridyl group in 4/3-Hcptpy can be confirmed. Indeed, the central pyridyl groups in all reported 4/3-Hcptpy complexes are uncoordinated.⁸ It is also discovered that the rigid 4/3-Hcptpy ligands normally can be simplified into three-connected and two-connected nodes as building blocks, acting as three-connected junctions for complexes **4**, **6** and **7**, and as two-connected knots in complexes **1**, **2**, **3** and **5**. We believe that this directed expansion capability will make 4/3-Hcptpy as good candidates for rational design and assembly of target complexes in the future work.

Scheme 2. The coordination modes of 4/3-Hcptpy in complexes 1-7



Syntheses and structural diversity. Complexes **1–7** were successfully prepared by hydro(solvo)thermal reactions. As mentioned above, self-assembly process can be heavily influenced by subtle changes of many factors. Through analysis and comparison, concerning the 4/3-Hcptpy system and their derived coordination polymers, some basic synthetic rules and structural features of the frameworks can be summed up as follows:

a) Due to the existence of the carboxyl group, the type and quantity of the alkaline reagent added in the reaction, in other words, the pH value of the entire system has an important impact on the final products. For example, a mixture of 4-Hcptpy and NaOH in 1:1 molar ratio reacts with Mn(II) salt produces a 3D metal–organic framework (complex **1**). However, reducing the pH value through changing the ratio of 4-Hcptpy/NaOH to 2:1 will give rise to an obviously different 2D Mn₃ polymeric network with flower-like pattern (complex **3**). Moreover, the deprotonated process of carboxyl acid can be conveniently completed by solvothermal reaction in DMF solution without any addition of base. For complex **4**, a 2D hexagonal honeycomb microporous framework was built in DMF solvent without alkaline reagent. We speculate that the decomposition of DMF at solvothermal conditions could produce basic compound Me₂NH, which promotes the deprotonation procedure of the carboxyl group in Hcptpy. Meanwhile, formate ligands were also observed in complexes **4** and **6**. Recently, Liu et al. prepared a complex (Me₂NH)₃[Mn₆(HEBDC)₄(H₂O)₈]·2DMF·H₂O in DMF solution at 105 °C. Obviously, Me₂NH is formed by the decomposition of DMF.¹⁴ Similar DMF decomposition behavior was also observed in complex (Me₂NH)₂[Cu₉(bshz)₃(Py)₁₀(C₂H₇N)(DMF)]·2DMF.¹⁵ This is why some carboxylate complexes were prepared in DMF solution without alkaline additive in recent research.¹⁶ In contrast with **4**, the solvothermal reaction of complex **5** in ethanol without alkaline additive afforded a 1D 2₁ helical chain structure, in which the carboxyl group remains protonated, thus restricting the extension of the architecture. It is well-known that metal-hydroxide precipitates are easily produced when preparing carboxylate complexes using NaOH and triethylamine as bases. Now we can prepare carboxylate complexes conveniently under solvothermal conditions in DMF solution without any basal additive.

b) Based on the intrinsic triangular rigid skeletons of 4/3-Hcptpy ligands, porous metal–organic frameworks are easy to be constructed. Hexagonal pores with various dimensions are found in complexes **1**, **2**, **4** and **5**. Additionally, the intermolecular π – π stacking interactions stemming from the large π -conjugated structures of the 4/3-Hcptpy ligands contribute a lot to the stability of the

supramolecular architectures of complexes **5** and **6**.

On the basis of the above observations, it can be found that the pH value, solvent, and the coordination character of 4/3-Hcptpy all have significant effects on the structures of the resulting coordination polymers. In addition to this, the synthetic strategy of complex **3** is being further optimized for looking forward to a better yield and further investigate its properties such as magnetic coupling.

Infrared spectra. The existences of 4/3-Hcptpy ligands in seven complexes were confirmed by IR spectroscopy (Fig. S5, ESI). The bands locate near 3070, 1600, and 1560 cm⁻¹ are assigned, respectively, to the stretching vibrations of C–H, C=C and C=N bonds of 4/3-cptpy. While bands near 825 and 780 cm⁻¹ can be designated to δ (C–H) bending vibrations of pyridyl and phenyl groups. The strong ν (COOH) absorption peak of **5** at 1685 cm⁻¹ indicates that the carboxyl group of 4-Hcptpy remains protonated. The carboxyl groups of 4/3-Hcptpy ligands in other six complexes are deprotonated.

Specifically, characteristic absorption bands at about 1600–1580 cm⁻¹ correspond to the asymmetric stretching vibrations of COO⁻ group, whereas those at about 1420–1400 cm⁻¹ are attributable to their symmetric vibrations. The separations between the $\nu_{as}(\text{COO})$ and $\nu_s(\text{COO})$ bands in **1**, **2** and **4** are all less than 200 cm⁻¹, which confirm the bidentate chelating mode of the carboxylate groups.¹⁷ In the IR spectrum of **4**, the strong absorption peak at 1662 cm⁻¹ is ascribed to the stretching vibration of carbonyl group (C=O) in lattice DMF molecule. In addition, the bands near 3450 cm⁻¹ are associated with the coordinated and lattice water molecules. These IR spectra are in good agreement with the results of elemental analyses and X-ray structural characterizations.

Thermogravimetric analyses. In order to investigate the thermal stabilities of 4-Hcptpy complexes, the thermal behaviors of complexes **1** and **2** are chosen to be tested by TG-DSC (Fig. S6, ESI). The experiments are performed on solid samples consisting of numerous single crystals in the 20–800 °C temperature range under N₂ atmosphere. Based on the isostructural frameworks of **1** and **2**, both complexes exhibit similar TG curves and maintain structural stabilities under 440 °C. In the 440–500 °C range, both complexes exhibit an explosive decomposition, corresponding to the loss of partial 4-cptpy⁻ ligands. The intermediates could be [Mn(ph-COO)₂] for **1** (found, 65.96%; calcd, 61.05%), and [Co(ph-COO)₂] for **2** (found, 66.13%; calcd, 60.56%). After that, the intermediates begin to decompose gradually in 520–620 °C, losing the remaining 4-cptpy⁻ ligands. The final residues are MnO₂ for **1** (found, 8.74%; calcd, 11.32%) and CoO for **2** (found,

8.07%; calcd, 9.81%).

Photoluminescence. Considering the large π -conjugated structure of rigid 4-Hcptpy ligand and the varied luminescent behaviors of d^{10} transition metal complexes,¹⁸ we investigate the luminescent behavior of Zn(II) complex **5** in the solid state at room temperature (Fig. 7). When excited with 329 nm light, the Zn(II) complex **5** acts as a strong violet luminescent emitter with an emission maximum at 383 nm. To understand the emission mechanism, the luminescence of 4-Hcptpy ligand is determined for comparison. With similar excitation at 329 nm, 4-Hcptpy exhibits an emission peak centered at 381 nm, assigned to the intraligand $\pi^* \rightarrow \pi$ transition. Therefore, similar emission energy between the tested complex and the 4-Hcptpy ligand indicates that the luminescent mechanism of **5** originates from ligand-centered emission. The enhancement of the intensity of **5** could be attributed to the unique coordination of 4-Hcptpy to the Zn(II) center, which increases the conformational rigidity of the ligand.

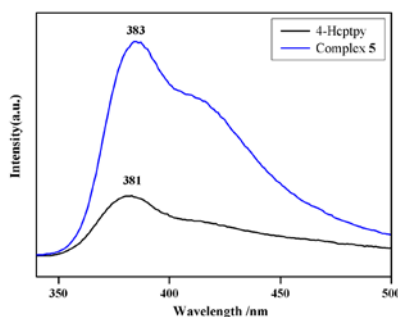


Fig. 7 Emission spectra of Zn(II) complex **5** and 4-Hcptpy ligand.

Magnetic properties. For the magnetic properties of cptpy complexes, Zhao et al. reported two novel 2D 3d-4f networks based on planar Co_4Ln_2 clusters supported by rigid 2-Hcptpy ligand, which perform single-molecule magnet behaviors.¹⁹ This finding promotes us to investigate the magnetic properties of 4-Hcptpy complexes **1** and **2**, which contain Mn_2 and Co_2 dimers.

The temperature dependence of magnetic susceptibilities of $[\text{Mn}(4\text{-cptpy})_2]_n$ (**1**) and $[\text{Co}(4\text{-cptpy})_2]_n$ (**2**) were measured in the temperature range of 2–300 K at a magnetic field of 1000 Oe. The variation of $\chi_{\text{M}}T$ versus T is plotted in Fig. 8. For complex **1**, the $\chi_{\text{M}}T$ value per Mn_2 unit at 300 K is $8.35 \text{ cm}^3 \cdot \text{K} \cdot \text{mol}^{-1}$, which is close to the spin-only value ($8.37 \text{ cm}^3 \cdot \text{K} \cdot \text{mol}^{-1}$ with $g = 2.0$) of two Mn^{2+} ions ($S = 5/2$). For complex **2**, the $\chi_{\text{M}}T$ value per Co_2 unit at 300 K is $5.72 \text{ cm}^3 \cdot \text{K} \cdot \text{mol}^{-1}$, which is also close to the value expected for spin-only value of two Co^{2+} ions ($5.48 \text{ cm}^3 \cdot \text{K} \cdot \text{mol}^{-1}$ with $g = 2.0$, $S = 3/2$).

Upon cooling of the sample from 300 to 2 K, the $\chi_{\text{M}}T$

value of complex **1** decreases continuously from 8.35 to $1.00 \text{ cm}^3 \cdot \text{K} \cdot \text{mol}^{-1}$. Considering that the Mn_2 cluster is isolated by larger 4-cptpy ligands, the appropriate magnetic exchange pathway in $(\mu\text{-O}_2\text{CR})_2\text{Mn}_2$ core is through the bidentate carboxylate bridges. Due to the magnetic couple is located at Mn_2 unit ($S_1 = S_2 = 5/2$), a theoretical susceptibility equation based on the spin Hamiltonian ($\mathbf{H} = -2J \mathbf{S}_1 \cdot \mathbf{S}_2$) is employed to evaluate the magnetic exchange constant by fitting the magnetic susceptibility data.²⁰ This gives the singlet-triplet energy separation value $J = -0.49 \text{ cm}^{-1}$, $g = 1.97$, and an agreement factor R of 1.62×10^{-2} . This result indicates the presence of weak antiferromagnetic interaction in the Mn_2 dimer. In the period of 38–50 K, the $\chi_{\text{M}}T$ value slightly increased by lowering the temperature, indicating a weak ferromagnetic coupling existing between adjacent Mn_2 dimers.

Complex **2** is isostructural with complex **1**, and has similar $\chi_{\text{M}}T$ - T curve. A theoretical susceptibility equation suitable for Co_2 unit ($S_1 = S_2 = 3/2$) is employed to evaluate the magnetic exchange constant by fitting the magnetic susceptibility data in 35–300 K.²¹ This gives the singlet-triplet energy separation value $J = -2.56 \text{ cm}^{-1}$, $g = 2.49$, and an agreement factor R of 3.12×10^{-4} . This result indicates a weak antiferromagnetic interaction existing in the Co_2 dimer.

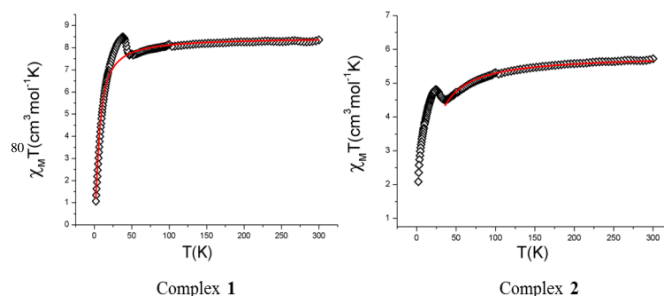


Fig. 8 The plots of $\chi_{\text{M}}T$ vs. T for **1** (left) and **2** (right). The solid red line represents the best theoretical fit.

Conclusions

Based on the rigid triangular-shaped 4/3-Hcptpy ligands, seven coordination polymers with dimensional diversity from 1D to 3D have been successfully prepared and structurally characterized. Among **1**–**7**, 4/3-Hcptpy ligands act as three- or two-connected nodes and present up to seven coordination modes. The detailed investigation reveals that the overall structures of complexes could be affected by multi-factors, such as pH value, solvent, and weak intermolecular interactions. A generally solvothermal method is proposed for preparing carboxylate complexes in DMF solution without any basal additive. Antiferromagnetic interactions were detected in the discrete

dinuclear Mn/Co clusters of complexes **1** and **2**, which also possess high thermal stabilities. Zn(II) complex **5** is confirmed to be a strong violet luminescent emitter. 4/3-Hcptpy ligands can be considered as two potential

Acknowledgments

This work was financially supported by National Natural Science Foundation of China (21171115, 21203117) and Innovation Program (12ZZ089) of Shanghai Municipal Education Commission.

Notes

†Electronic Supplementary Information (ESI) available: Selected bond distances and angles, IR spectra and TGA curves. CCDC reference numbers 943673–943677, 943680 and 943681. For ESI and crystallographic data in CIF or other electronic format see DOI: 10.1039/b000000x/

References

- (a) H. C. Zhou, J. R. Long, O. M. Yaghi, *Chem. Rev.* 2012, **112**, 673. (b) D. J. Tranchemontagne, J. L. Mendoza-Cortes, M. O'Keeffe, O. M. Yaghi, *Chem. Soc. Rev.* 2009, **38**, 1257. (c) T. R. Cook, Y. R. Zheng, P. J. Stang, *Chem. Rev.* 2013, **113**, 734. (d) J. J. Perry, J. A. Perman, M. J. Zaworotko, *Chem. Soc. Rev.* 2009, **38**, 1400. (e) N. Ye, C. Tu, X. Long, M. Hong, *Cryst. Growth Des.* 2010, **10**, 4672. (f) M. C. Munoz, J. A. Real, *Coord. Chem. Rev.* 2011, **255**, 2068. (g) G. C. Xu, W. Zhang, X. M. Ma, Y. H. Chen, L. Zhang, H. L. Cai, Z. M. Wang, R. G. Xiong, S. Gao, *J. Am. Chem. Soc.* 2011, **133**, 14948. (h) G. Férey, *Chem. Soc. Rev.* 2008, **37**, 191. (i) Z. Z. Lu, R. Zhang, Y. Z. Li, Z. J. Guo, H. G. Zheng, *J. Am. Chem. Soc.* 2011, **133**, 4172.
- (a) J. P. Zhang, Y. B. Zhang, J. B. Lin, X. M. Chen, *Chem. Rev.* 2012, **112**, 1001. (b) W. Xuan, C. Zhu, Y. Liu, Y. Cui, *Chem. Soc. Rev.* 2012, **41**, 1677. (c) S. Kitagawa, R. Kitaura, S. Noro, *Angew. Chem., Int. Ed.* 2004, **43**, 2334. (d) R. E. Morris, X. H. Bu, *Nature Chem.* 2010, **2**, 353. (e) D. Dang, P. Wu, C. He, Z. Xie, C. Duan, *J. Am. Chem. Soc.* 2010, **132**, 14321. (f) M. X. Li, H. Wang, S. W. Liang, M. Shao, X. He, Z. X. Wang, S. R. Zhu, *Cryst. Growth Des.* 2009, **9**, 4626. (g) T. F. Liu, J. Lu, R. Cao, *CrystEngComm*, 2010, **12**, 660. (i) Q. Yang, Z. Chen, J. Hu, Y. Hao, Y. Li, Q. Lu, H. Zheng, *Chem. Commun.* 2013, **49**, 3585. (h) X. Zhu, P. P. Sun, J. G. Ding, B. L. Li, H. Y. Li, *Cryst. Growth Des.* 2012, **12**, 3992.
- (a) Z. G. Guo, R. Cao, *J. Am. Chem. Soc.* 2009, **131**, 6894. (b) S. Q. Zang, M. M. Dong, Y. J. Fan, H. W. Hou, T. C. W. Mak, *Cryst. Growth Des.* 2012, **12**, 1239. (c) X. He, X. P. Lu, Z. F. Ju, C. J. Li, Q. K. Zhang, M. X. Li, *CrystEngComm* 2013, **15**, 2731. (d) C. P. Li, M. Du, *Chem. Commun.* 2011, **47**, 5958. (e) M. Yang, F. Jiang, Q. Chen, Y. Zhou, R. Feng, K. Xiong, M. Hong, *CrystEngComm* 2011, **13**, 3971.
- (a) N. N. Adarsh, P. Dastidar, *Chem. Soc. Rev.*, 2012, **41**, 3039. (b) C. Janiak, J. K. Vieth, *New J. Chem.* 2010, **34**, 2366. (c) O. M. Yaghi, H. Li, C. Davis, D. Richardson, T. L. Groy, *Acc. Chem. Res.* 1998, **31**, 474.
- (a) L. Hammarstroem, O. Johansson, *Coord. Chem. Rev.* 2010, **254**, 2546. (b) K. K. W. Lo, S. P. Y. Li, K. Y. Zhang, *New J. Chem.* 2011, **35**, 265. (c) W. Huang, W. You, L. Wang, C. Yao, *Inorg. Chim. Acta* 2009, **362**, 2127. (d) M. Fujita, M. Tominaga, A. Hori, B. Therrien, *Acc. Chem. Res.* 2005, **38**, 369. (d) M. X. Li, Z. X. Miao, M. Shao, S. W. Liang, S. R. Zhu, *Inorg. Chem.* 2008, **47**, 4481.
- (a) M. W. Cooke, G. S. Hanan, F. Loiseau, S. Campagna, M. Watanabe, Y. Tanaka, *J. Am. Chem. Soc.* 2007, **129**, 10479. (b) A. Stublla, P. G. Potvin, *Eur. J. Inorg. Chem.* 2010, 3040. (c) M. W. Cooke, P. M. Tremblay, G. S. Hanan, *Inorg. Chem. Commun.* 2007, **10**, 1365. (d) E. C. Constable, E. L. Dunphy, C. E. Housecroft, M. Neuburger, S. Schaffner, F. Schaper, S. R. Batten, *Dalton Trans.* 2007, 4323.
- (a) D. C. Goldstein, Y. Y. Cheng, T. W. Schmidt, M. Bhadbhade, P. Thordarson, *Dalton Trans.* 2011, **40**, 2053. (b) P. Sinha, D. S. Raghuvanshi, K. N. Singh, L. Mishra, *Polyhedron*, 2012, **31**, 227. (c) Q. R. Wu, J. J. Wang, H. M. Hu, Y. Q. Shanguan, F. Fu, M. L. Yang, F. X. Dong, G. L. Xue, *Inorg. Chem. Commun.* 2011, **14**, 484.
- (a) L. Wen, X. Ke, L. Qiu, Y. Zou, L. Zhou, J. Zhao, D. Li, *Cryst. Growth Des.* 2012, **12**, 4083. (b) C. Niu, A. Ning, C. Feng, X. Wan, C. Kou, *J. Inorg. Organomet. Polym.* 2012, **22**, 519. (c) N. Li, Q. E. Zhu, H. M. Hu, H. L. Guo, J. Xie, F. Wang, F. X. Dong, M. L. Yang, G. L. Xue, *Polyhedron*, 2013, **49**, 207. (d) Y. L. Gai, F. L. Jiang, L. Chen, Y. Bu, M. Y. Wu, K. Zhou, J. Pan, M. C. Hong, *Dalton Trans.* 2013, **42**, 9954.
- G.M. Sheldrick, *SHELXTL*. Version 6.1; Bruker AXS Inc., Madison, Wisconsin, USA, 2000.
- (a) N. Taleb, V. J. Richards, S. P. Argent, J. van Slageren, W. Lewis, A. J. Blake, N. R. Champness, *Dalton Trans.* 2011, **40**, 5891. (b) P. Alborés, E. Rentschler, *Dalton Trans.* 2010, **39**, 5005.
- (a) Y. Ma, K. Wang, E. Q. Gao, Y. Song, *Dalton Trans.* 2010, **39**, 7714. (b) M. Wang, C. B. Ma, H. S. Wang, C. N. Chen, Q. T. Liu, *J. Mol. Struct.* 2008, **873**, 94. (c) H. H. Zou, S. H. Zhang, M. H. Zeng, Y. L. Zhou, H. Liang, *J. Mol. Struct.* 2008, **885**, 50.
- N. Bao, L. Shen, G. Srinivasan, K. Yanagisawa, A. Gupta, *J. Phys. Chem. C* 2008, **112**, 8634.
- (a) F. Dai, D. Sun, D. Sun, *Cryst. Growth Des.* 2011, **11**, 5670. (b) P. J. Calderone, D. Banerjee, A. M. Plonka, S. J. Kim, J. B. Parise, *Inorg. Chim. Acta*, 2013, **394**, 452. (c) L. Liu, Z. G. Ren, L. W. Zhu, H. F. Wang, W. Y. Yan, J. P. Lang, *Cryst. Growth Des.* 2011, **11**, 3479.
- B. Zheng, J. Luo, F. Wang, Y. Peng, G. Li, Q. Huo, Y. Liu, *Cryst. Growth Des.* 2013, **13**, 1033.
- D. Liu, Z. Chen, W. Huang, S. Qin, L. Jiang, S. Zhou, F. Liang, *Inorg. Chim. Acta* 2013, **400**, 179.
- (a) Y. S. Xue, F. Y. Jin, L. Zhou, M. P. Liu, Y. Xu, H. B. Du, M. Fang, X. Z. You, *Cryst. Growth Des.* 2012, **12**, 6158.

- (b) A. D. Burrows, K. Cassar, T. Düren, R. M. W. Friend, M. F. Mahon, S. P. Rigby, T. L. Savarese, *Dalton Trans.* 2008, 2465.
- 17 G. B. Deacon, R. J. Phillips, *Coord. Chem. Rev.* 1980, **33**, 227.
- 18 (a) M. D. Allendorf, C. A. Bauer, R. K. Bhakta, R. J. T. Houk, *Chem. Soc. Rev.* 2009, **38**, 1330. (b) G. Q. Kong, C. D. Wu, *Cryst. Growth Des.* 2010, **10**, 4590. (c) Q. R. Wu, J. J. Wang, H. M. Hu, B. C. Wang, X. L. Wu, F. Fu, D. S. Li, M. L. Yang, G. L. Xue, *Inorg. Chem. Commun.* 2010, **13**, 715.
- 19 Y. Liu, Z. Chen, J. Ren, X. Q. Zhao, P. Cheng, B. Zhao, *Inorg. Chem.* 2012, **51**, 7433.
- 20 D. Luneau, J. M. Savariault, P. Cassoux, J. P. Tuchagues, *J. Chem. Soc. Dalton Trans.*, 1988, 1225.
- 21 P. W. Ball, A. B. Blake, *J. Chem. Soc. Dalton Trans.*, 1974, 852.

Table 1. Crystallographic data and structure refinement for complexes 1–7

	1	2	3
formula	C ₄₄ H ₂₈ N ₆ O ₄ Mn	C ₄₄ H ₂₈ N ₆ O ₄ Co	C ₁₃₂ H ₉₀ N ₁₈ O ₁₅ Mn ₃
fw	759.66	763.65	2333.05
cryst syst	monoclinic	monoclinic	triclinic
space group	<i>P2₁/c</i>	<i>P2₁/c</i>	<i>P</i> $\bar{1}$
<i>a</i> (Å)	9.299(12)	9.456(8)	10.644(1)
<i>b</i> (Å)	21.109(3)	20.560(18)	17.496(2)
<i>c</i> (Å)	19.378(2)	19.480(15)	30.022(3)
α (deg)	90	90	98.411(2)
β (deg)	104.356(5)	105.539(3)	91.251(2)
γ (deg)	90	90	96.172(2)
<i>V</i> [Å ³]	3685.1(8)	3648.8(5)	5494.9(10)
<i>Z</i>	4	4	2
<i>D_c</i> (g cm ⁻³)	1.369	1.390	1.410
μ (mm ⁻¹)	0.411	0.524	0.418
reflections/ unique	19096/6511	22740/8367	36209/21392
<i>R</i> _{int}	0.0821	0.0605	0.0557
data/restraints /params	6511/0/496	8367/0/496	21392/103/1491
GOF on <i>F</i> ²	1.113	1.236	1.030
<i>R</i> ₁ , <i>wR</i> ₂ (<i>I</i> > 2 σ (<i>I</i>))	0.0625, 0.0888	0.0524, 0.0709	0.1036, 0.2783
largest diff. peak and hole (e Å ⁻³)	0.358, -0.388	0.291, -0.377	1.170, -1.051

4	5	6	7
C ₂₆ H ₂₄ N ₄ O ₆ Co	C ₄₈ H ₄₄ Cl ₄ N ₆ O ₇ Zn ₂	C ₉₂ H ₆₄ N ₁₂ O ₁₈ Co ₄	C ₄₄ H ₂₈ N ₆ O ₄ Mn
547.42	1089.43	1861.27	759.66
monoclinic	orthorhombic	triclinic	triclinic
<i>P2₁/n</i>	<i>Pnna</i>	<i>P</i> $\bar{1}$	<i>P</i> $\bar{1}$
7.291(1)	16.766(1)	11.702(1)	9.962(4)
26.677(5)	14.069(1)	18.389(2)	10.641(4)
12.932(2)	20.444(2)	20.506(3)	17.524(7)
90	90	113.866(1)	86.709(5)
106.170(2)	90	101.406(2)	79.071(5)
90	90	95.164(2)	66.811(3)

2415.7(7)	4822.7(8)	3883.8(9)	1676.3(11)
4	4	2	2
1.505	1.500	1.592	1.505
0.761	1.274	0.925	0.452
14165/5452	23767/4271	24369/17112	10495/7349
0.0698	0.0362	0.0187	0.0244
5452/0/336	4271/1/287	17112/0/1135	7349/102/496
1.143	1.041	1.021	1.406
0.0938, 0.1647	0.0478, 0.1287	0.0410, 0.0998	0.1111, 0.3386
0.465, -0.807	0.677, -0.896	0.561, -0.309	3.387, -0.751
